

Filament Shape Versus Coronal Potential Magnetic Field Structure

B. Filippov ^{*}

Pushkov Institute of Terrestrial Magnetism, Ionosphere and Radio Wave Propagation of the Russian Academy of Sciences (IZMIRAN), Troitsk, Moscow 142190, Russia

Accepted 0000 December 15. Received 0000 December 14; in original form 0000 October 11

ABSTRACT

Solar filament shape in projection on disc depends on the structure of the coronal magnetic field. We calculate the position of polarity inversion lines (PILs) of coronal potential magnetic field at different heights above the photosphere, which compose the magnetic neutral surface, and compare with them the distribution of the filament material in $H\alpha$ chromospheric images. We found that the most of the filament material is enclosed between two polarity inversion lines (PILs), one at a lower height close to the chromosphere and one at a higher level, which can be considered as a height of the filament spine. Observations of the same filament on the limb by the *STEREO* spacecraft confirm that the height of the spine is really very close to the value obtained from the PIL and filament border matching. Such matching can be used for filament height estimations in on-disk observations. Filament barbs are housed within protruding sections of the low-level PIL. On the base of simple model, we show that the similarity of the neutral surfaces in potential and non-potential fields with the same sub-photospheric sources is the reason for the found tendency for the filament material to gather near the potential-field neutral surface.

Key words: Sun: activity – Sun: filaments, prominences – Sun: magnetic fields.

1 INTRODUCTION

Solar prominences are ‘clouds’ of cooler and denser plasma in the much hotter and rarefied solar corona. Most of them look like long dark ‘filaments’ in strong spectral lines due to absorption of the background radiation when they are projected on the solar disk. Quiescent prominences (filaments) frequently take the form of thin ribbons or curtains. The typical thickness of the ribbons (5–6 Mm) is much smaller than both their height (30–35 Mm) and their length along the solar surface (> 200 Mm) (d’Azambuja & d’Azambuja 1948; Tandberg-Hanssen 1974; Rompolt 1990; Mackay et al. 2010; Parenti 2014). Filament locations on the Sun reflect their magnetic origin. Comparisons with maps of the photospheric magnetic field show that filaments are always located above lines separating opposite polarities of the radial field, polarity inversion lines (PIL) sometimes called neutral lines (Babcock & Babcock 1955; Howard & Harvey 1964; Smith & Ramsey 1967; McIntosh 1972).

A region surrounding a PIL forms an inversion zone that corresponds to the filament channel. A simple potential extrapolation of the photospheric field yields an arcade of loops in this inversion zone. The magnetic field-lines di-

rectly above the inversion line should be horizontal and predominantly transverse to this line. In fact, the field in the filament channel is much more complex. Zeeman (Zirin & Severny 1961; Rust 1967; Ioshpa 1968; Tandberg-Hanssen 1970; Kim 1990) and Hanle (Leroy 1977, 1978; Bommier et al. 1994; Bommier & Leroy 1998) effect measurements of the magnetic fields in prominences have shown that, as a rule, the field in the channel is horizontal, but directed nearly along the filament axis and PIL. The angle to the axis is 25° , on average. Moreover, the component transverse to the axis is predominantly opposite to that calculated in the potential approximation.

To support stably heavy cool plasma against gravity, a magnetic field lines should be locally horizontal and curved upward, i.e., should contain dips in the field line shapes (Kippenhahn & Schlüter 1957). In particular, dips are present in a potential field with a quadrupolar structure of underlying photospheric magnetic sources. However, many observational details indicate that the magnetic fields in filament channels are not potential and contain significant electric currents. Two non-potential magnetic configurations are usually considered as possible ‘magnetic skeleton’ of filaments. Magnetic flux ropes with nearly force-free field that lie horizontally above the PIL have dips in lower parts of helical field lines (Kuperus & Raadu 1974; Pneuman 1983;

* E-mail: bfilip@izmiran.ru

van Ballegoijen & Martens 1989; Priest et al. 1989; Rust & Kumar 1994; Aulanier & Démoulin 1998; Chae et al. 2001; Gibson & Fan 2006). Sheared arcades are also proposed as magnetic structures of the filament channels (Antiochos et al. 1994; DeVore & Antiochos 2000; Aulanier et al. 2006).

Typically 3 major structural components can be recognized in a filament, namely a spine, barbs, and two extreme ends. The spine is a nearly horizontal line along the top of the filament. The barbs or intermediate 'legs' of the filament protrude from its main body on both sides. The barbs look to connect the spine to the chromosphere below, when the filament is observed closer to the limb.

When observed from above, the filament barbs are seen to protrude at an acute angle either clockwise or counter-clockwise with respect to the axis of the filament (Martin et al. 1994). Depending on the deviation of the barbs, filaments were classified as either right-bearing or left-bearing. In exactly the same way, filaments can be classified as dextral or sinistral depending on the direction of the axial component of the field to the right or to the left, when viewed from the major photospheric positive polarity (Martin et al. 1994). This handedness property was called 'chirality' (Martin 1998). Martin and collaborators found that dextral filaments have always right-bearing barbs, while sinistral filaments have left-bearing barbs.

Many authors studied the relationship between the position of the filament barbs and the underlying photospheric magnetic field. Some results are contradictory possibly because the real height of the barb endpoints is uncertain in on-disk observations. Plocieniak & Rompolt (1973) found that most of filament feet are clustered in junctions of three or more adjacent supergranular cells, where the concentration of vertically oriented field is the largest. Martin et al. (1994) and van Ballegoijen (2004) believed that the ends of the barbs are connected to weak magnetic fields in between the network elements. Martin & Echols (1994) found that the barbs are anchored in parasitic (minority) polarity elements. Wang (1999, 2001), Chae et al. (2005), and Lin et al. (2005) showed that the barbs are ended very close to small-scale PILs between majority and minority polarities on the side of the filament.

Since the vertical size of barbs is much larger than the gravitational scale height of the prominence plasma, the barbs cannot be static structures within inclined flux tubes. The prominence plasma must somehow resist to falling down to the chromosphere or the prominence must be a non-equilibrium dynamic formation. Therefore, the structure of barbs and the orientation of the magnetic field in them are key issues. Aulanier and collaborators (Aulanier & Démoulin 1998; Aulanier et al. 1998, 1999) developed a model of three-dimensional magnetic configuration of filaments based on the idea of magnetic dips, which successfully reproduced the general shape of filaments. They used either linear force-free fields or linear magnetohydrostatic fields. Plasma of the main body of the filament is supported at local dips in the bottom part of the helical windings of a coronal flux rope. Barbs are formed in small dips above minor photospheric polarity inversion lines around magnetic elements whose polarity is opposite to the dominant polarity of surrounding magnetic fields. van Ballegoijen (2004) constructed a three-dimensional magnetic model of a filament using a nonlinear force-free configuration. The initial flux rope was subjected

to magnetofrictional relaxation. The dips in the helical field lines are formed under the influence of neighboring network elements. The model reproduces the observed filament barb.

A photospheric PIL is the intersection of the surface $B_r = 0$, which can be called a 'neutral surface', with the photosphere. Zagnetko et al. (2005) found that filaments not only follow photospheric PILs but most of the filament material is concentrated close to the neutral surface or surface passing through apices of arches of potential magnetic field-lines. This property possibly appears due to the fact that, while the neutral surface is not as a rule the location of dips, it is a place where coronal currents can find horizontal equilibrium. The axis of the flux rope containing a filament should lie in the neutral surface and after the lost of equilibrium during an eruption, the flux rope some time moves along the neutral surface (Filippov et al. 2001, 2002; Filippov 2013a, 2015a).

In this paper, we compare in more detail the shape of filaments and the shape of neutral surfaces calculated in potential approximation on the base of photospheric magnetograms. From this comparison we are able to determine the height of filament spines in on-disk observations. The results are verified by simultaneous on-limb observations from a different viewpoint. Folds of the neutral surface near the chromosphere revealed by projections of low-altitude PILs are possible locations of filament barbs.

2 DATA AND METHOD OF ANALYSIS

We used full-disk $H\alpha$ filtergrams from the archive of the Big Bear Solar Observatory for selecting rather wide filaments with conspicuously protruding barbs when they were located not far from the center of the solar disk or at least of the central meridian. This limitation arises from necessity to have good magnetographic data for a boundary condition in coronal magnetic field calculations. Polar crown filaments, which often have prominent barbs, are not likely for this purpose because photospheric magnetic field measurements are too noisy in polar regions.

Fig. 1a represents a fragment of the magnetogram taken by the Heliospheric and Magnetic Imager (HMI; Schou et al. (2012) on board the *Solar Dynamic Observatory (SDO)* on 2012 February 23 at 20:21 UT, which was used as the boundary condition for the potential magnetic field calculations. We need the potential magnetic field distribution in the corona at heights of prominences, which are much less than a solar radius. Therefore, we can use a restricted area of a photospheric magnetogram as the boundary of the calculation domain and neglect its sphericity considering it as a part of a flat surface (Filippov & Den 2000, 2001; Filippov 2013a). When we cut out a rectangular area around the filament under study from the full disk magnetogram, we ignore the contribution of the magnetic sources outside of it. Such simplification is reasonable if the main sources of the field lie within the cut-out area. For regions rather far from the center of the solar disk, we construct the data array with the equal angular size of pixels and assume the projection of the line-of-sight-field on the normal as the radial component. Thus we obtain the boundary condition for the calculation of the potential magnetic field as if the region were located at the center of the disk.

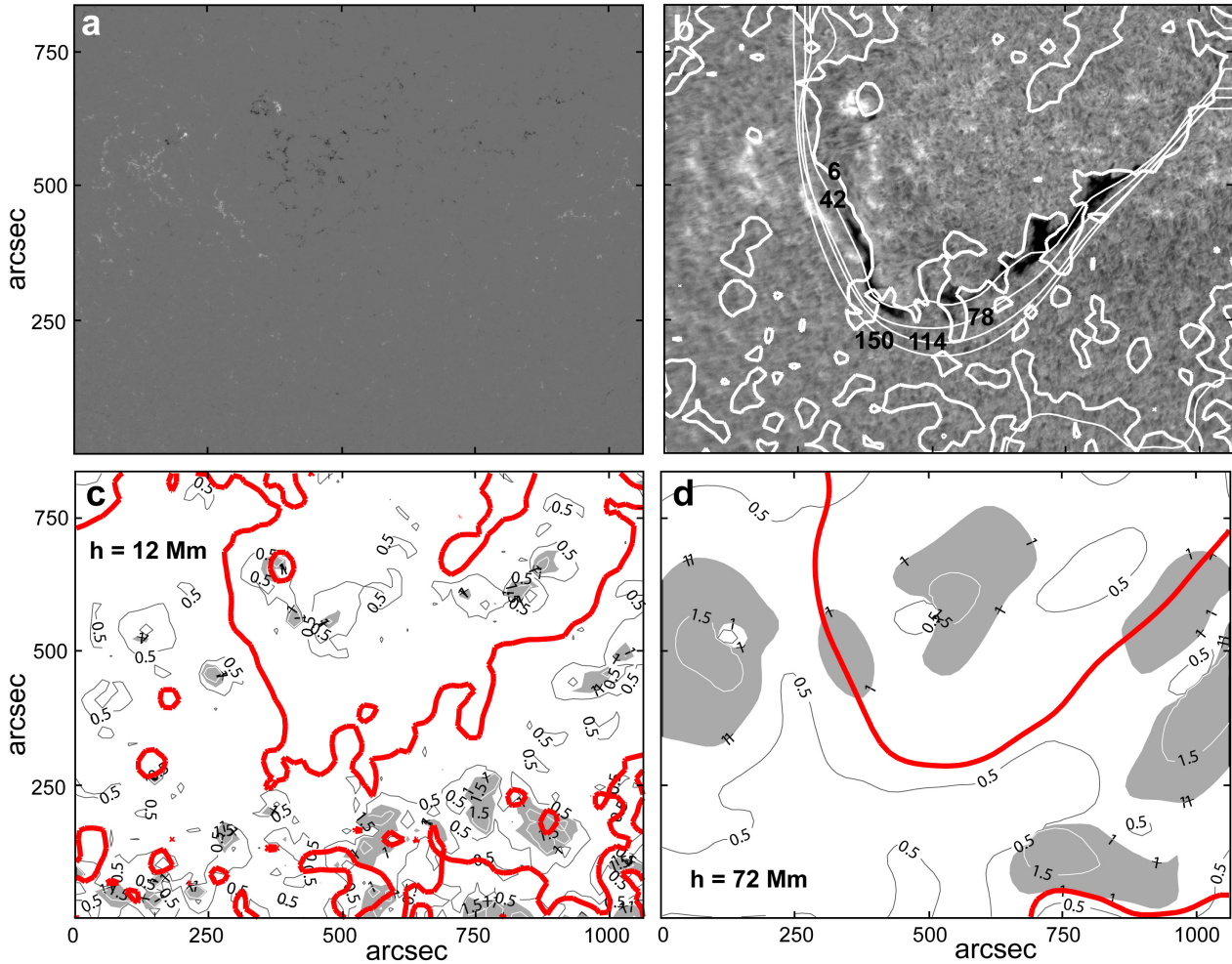


Figure 1. (a) HMI magnetogram of the region taken around the filament on 2012 February 23 at 20:21 UT. (Courtesy of the NASA/*SDO* and the HMI science team). (b) $H\alpha$ filtergram of the same region and at the same time with superposed PILs at a height of 6 (thicker lines), 42, 78, 114, and 150 Mm (thinner lines from top to bottom). (Courtesy of the Big Bear Solar Observatory), (c) - (d) Distributions of the decay index and PILs (thick red lines) at two heights. Shaded areas show the regions where $n > 1$.

We calculate B_z maps (z -axis is vertical) at different heights and obtain a set of PILs $B_z = 0$ as shown in Fig. 1b. This set of curves represents the neutral surface nearby the filament. More precisely, the set of curves shows the projection of the neutral surface on the plane of the photosphere. Each curve is the intersection of the surface $B_z = 0$ with a plane $z = \text{const}$. We choose the lowest level as the level of the middle chromosphere (~ 5 Mm) in order to have a rather smooth PIL without influence of small-scale fields. To take into account the angle between the local vertical with the line-of-sight, each PIL is displaced in a map along the x and y coordinates at distances

$$\Delta x = h \tan \lambda_0, \quad (1)$$

$$\Delta y = h \tan \varphi_0, \quad (2)$$

where h is the height of the PIL above the photosphere, λ_0 is the longitude of the center of the area, φ_0 is the latitude of it.

The set of curves we superpose on the $H\alpha$ filtergram of the same region as was selected for the magnetic field calculations (Fig. 1b). We choose a curve nearest to the fil-

ament spine. Most of filament material is located between the lowest PIL and the PIL that we believe correspond to the height of the filament spine. For the filament shown in Fig. 1b this is the PIL at a height of 60 Mm.

To be sure that the filament can be in stable equilibrium at the height that we obtain for the filament spine (60 Mm), we calculate the distribution of the decay index (Filippov & Den 2000, 2001; Filippov 2013a)

$$n = -\frac{\partial \ln B_t}{\partial \ln h}, \quad (3)$$

of the horizontal potential magnetic field B_t in this region at different heights h (Figs 1c-d) and find that the decay index is less than unity at the PILs up to the height of 70 Mm. Therefore, the flux rope containing the filament can be in stable equilibrium if its axis, which usually corresponds to the filament spine, is below this height.

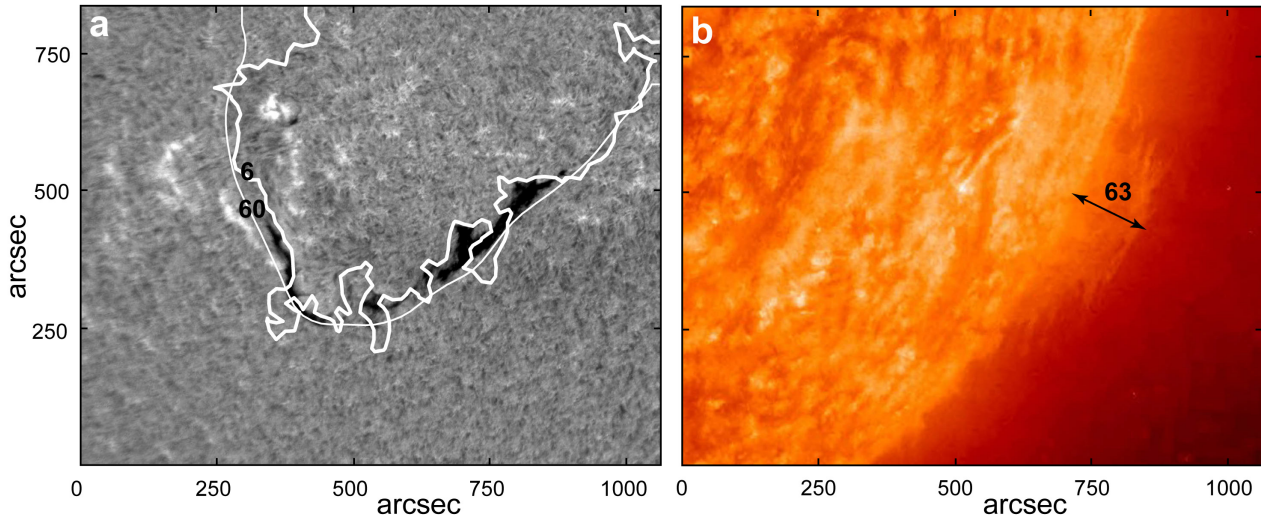


Figure 2. (a) The same H α filtergram as in Fig. 1b with superposed PILs related to the filament at heights of 6 (thicker line) and 60 Mm (thinner line). (Courtesy of the Big Bear Solar Observatory) (b) The same filament observed with *STEREO B/SECCHI EUVI 304-Å* on the limb on 2012 February 21 at 12:06 UT. (Courtesy of the *STEREO/SECCHI* Consortium.)

3 FILAMENT SHAPES AND POLARITY INVERSION LINES

3.1 Filament on 2012 February 23

Fig. 2a shows the same H α filtergram as in Fig. 1b with superposed PILs at a height of 6 and 60 Mm. In all figures in this section, we remove for clarity all PIL laying outside the filaments and show only PILs closest to the filaments on both sides (compare Fig. 2a and Fig. 1b). The PIL at the height of 60 Mm is nearest the filament spine. We can conclude that the height of the spine is about 60 Mm. This is the case because the filament was observed on the limb with the Sun Earth Connection Coronal and Heliospheric Investigation (SECCHI) EUVI (Wuelser et al. 2004; Howard et al. 2008) on board the *Solar Terrestrial Relations Observatory Behind (STEREO B)* on 2012 February 21 and with the identical instrument on board *STEREO Ahead (A)* on 2012 February 24. The separation angle with the Earth was 109° for *STEREO A* and 117° for *STEREO B*. The height of the highest point of the prominence spine (Fig. 2b) measured above the limb is 63 Mm on both days.

The whole filament body in Fig. 2a is enclosed between the 6 and 60 Mm PILs. While the filament spine is aligned with the smooth PIL at the height of 60 Mm, filament barbs are located between the PILs. Ends of barbs touch protruding sections of the PIL at the height of 6 Mm. This corresponds to their small heights above the chromosphere. The low-altitude PIL outlines roughly the barbs. However not all PIL protrusions are filled with filament barbs. Since the filament is located at middle latitude in the southern hemisphere, only barbs on the northern side of the filament are visible.

3.2 Filament on 2013 March 13

A filament with the straight spine stretched from the north-east to the south-west at middle latitudes in the northern hemisphere was observed near the central meridian on 2013

March 13. The spine fits best the PIL at a height of 48 Mm (Fig. 3a). Barbs on the southern side of the filament fill the space between this PIL and the PIL at a height of 6 Mm. The spine deviates from the 48 Mm PIL at the southern end, possibly because the height of the spine descends there. The height of the spine measured on the limb in the *STEREO B/SECCHI EUVI 304-Å* image on 2013 March 09 at 11:46 UT is 40 Mm (Fig. 3d). Distribution of the decay index indicates that the filament is stable up to a height of 75 Mm (Figs 3b-c).

3.3 Filament on 2013 January 31 in the southern hemisphere

Two wide filaments were located close to the central meridian not far from the equator in the southern and northern hemispheres on 2013 January 31. Both filaments have specific triangular barbs and thin spines.

The southern filament has three prominent barbs (Fig. 4a), which are enclosed between PILs at heights of 24 and 96 Mm. Lower than 24 Mm PILs deviate too far from the filament. The height of the spine measured on the limb in the *STEREO B/SECCHI EUVI 304-Å* image on 2013 January 28 at 11:26 UT is about 70 Mm (Fig. 4d). This value is 27% less than our estimation of the spine height from Fig. 4a. Figs 4b-c indicate that the filament is stable up to the height of 135 Mm.

3.4 Filament on 2013 January 31 in the northern hemisphere

In contrast to the southern filament, the filament in the northern hemisphere is low one. Its spine fits better to the PIL at a height of only 36 Mm (Fig. 5a). The height of a faint prominence observed on limb by the *STEREO B* on 2013 January 27 at 21:06 UT is 28 Mm (Fig. 5b). This value is again 22% less than our estimation of the spine height obtained from the superposition of the PILs and filtergram.

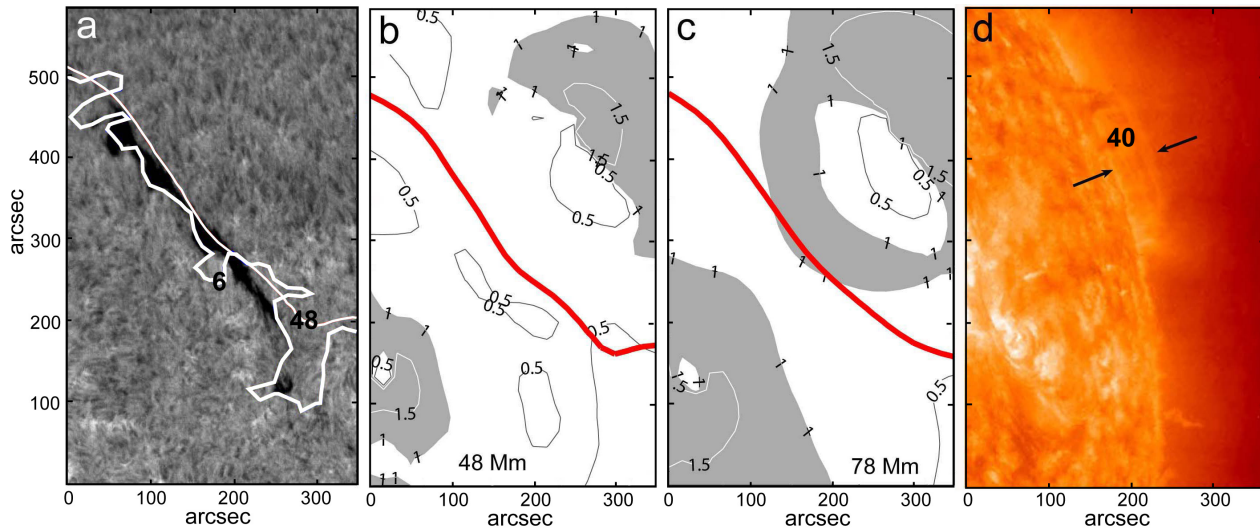


Figure 3. (a) $H\alpha$ filtergram of the filament on 2013 March 13 at 16:14 UT with superposed PILs related to the filament at heights of 6 (thicker line) and 48 Mm (thinner line). (Courtesy of the Big Bear Solar Observatory). (b) - (c) Distributions of the decay index and PILs (thick red lines) at different heights. Shaded areas show the regions where $n > 1$. (d) The same filament observed with *STEREO B/SECCHI EUVI 304-Å* on the limb on 2013 March 09 at 11:46 UT. (Courtesy of the *STEREO/SECCHI* Consortium.)

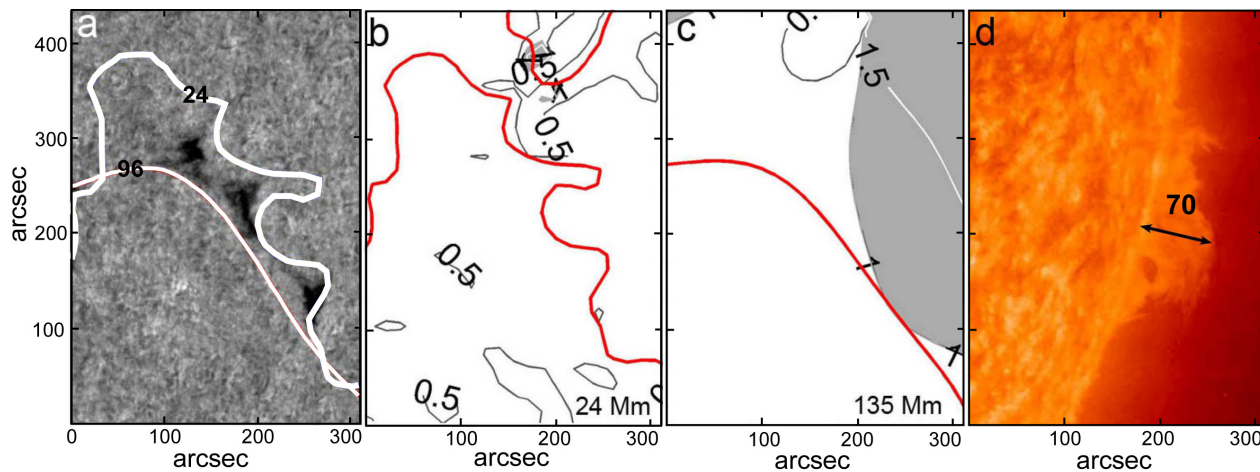


Figure 4. $H\alpha$ filtergram of the filament on 2013 January 31 at 20:38 UT with superposed PILs related to the filament at heights of 24 (thicker line) and 96 Mm (thinner line). (Courtesy of the Big Bear Solar Observatory). (b) - (c) Distributions of the decay index and PILs (thick red lines) at different heights. (d) The same filament observed with *STEREO B/SECCHI EUVI 304-Å* on the limb on 2013 January 28 at 11:26 UT. (Courtesy of the *STEREO/SECCHI* Consortium.)

As it follows from Fig. 5d, instability may also happen at a rather low height of 48 Mm.

4 NEUTRAL SURFACE IN A PRESENCE OF A FLUX ROPE

Examples presented in the previous section show that the filament material, as it seem in projection on the disk, fills the space between two PILs, one at a lower height and the other at a height of the filament spine. Therefore, the filament material is distributed near the coronal neutral surface. It seems natural because a part of the neutral surface where field-line curvature is directed upward is the location of dipo. However, we calculate only potential part of the coronal field, which is significantly different from the real coronal field

near filaments. Why does the potential-field neutral surface control the distribution of the filament plasma?

Let us consider a simple 2D model of electric current equilibrium in the coronal magnetic field. It was developed basing on the idea of van Tend & Kuperus (1978) by Molodenskii & Filippov (1987) for sub-photospheric magnetic sources represented by a vertical dipole and by Priest & Forbes (1990) for sources represented by a horizontal dipole. If the line electric current I is directed along the horizontal axis y and the z -axis is vertical, it generates a magnetic field in the upper hemisphere above a rigid conducting surface

$$B_x^I = \frac{2I}{c} \left(\frac{z-h}{x^2+(z-h)^2} - \frac{z+h}{x^2+(z+h)^2} \right), \quad (4)$$

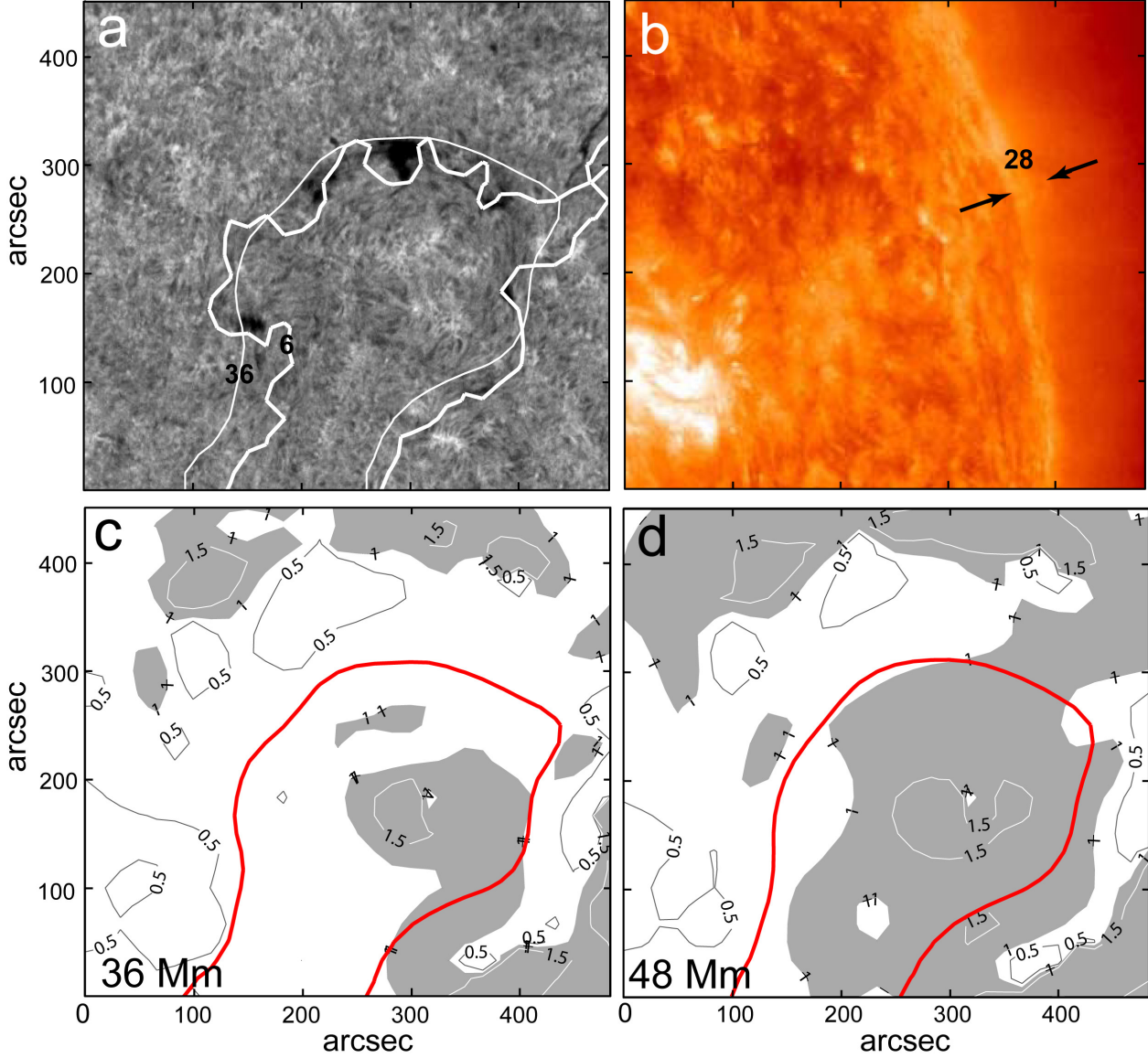


Figure 5. $H\alpha$ filtergram of the filament on 2013 January 31 at 20:38 UT with superposed PILs related to the filament at heights of 6 (thicker line) and 36 Mm (thinner line). (Courtesy of the Big Bear Solar Observatory). (b) The same filament observed with *STEREO* B/SECCHI EUVI 304-Å on the limb on 2013 January 27 at 21:06 UT. (Courtesy of the *STEREO*/SECCHI Consortium.) (c) - (d) Distributions of the decay index and PILs (thick red lines) at different heights.

$$B_z^I = -\frac{2Ix}{c} \left(\frac{1}{x^2 + (z-h)^2} - \frac{1}{x^2 + (z+h)^2} \right), \quad (5)$$

where $(0, h)$ are coordinates of the current

Possibly more relevant to typical solar conditions is the coronal magnetic field created by two sub-photospheric 'charges' $\pm q$ (Filippov, 2013b)

$$B_x^q = q \left(\frac{x+a}{(x+a)^2 + (z+d)^2} - \frac{x-a}{(x-a)^2 + (z+d)^2} \right), \quad (6)$$

$$B_z^q = q \left(\frac{z+d}{(x+a)^2 + (z+d)^2} - \frac{z+d}{(x-a)^2 + (z+d)^2} \right), \quad (7)$$

where $\pm a$ are the x -coordinates of the 'charges', d is the depth below the surface of the photosphere $z = 0$. The electric current is in equilibrium if

$$I = \frac{2qahc}{a^2 + (h+d)^2}. \quad (8)$$

Fig. 6a shows the shape of field lines for $q = 3$, $a = 1.5$, $d = 1$, $h = 1$ in dimensionless units. Dips exist at bottoms of nearly circular field lines below the current location. Their locus is the vertical line $x = 0$, where $B_z = 0$. All filament material should be close to the symmetry plane. Obviously, that the neutral surface (line in this 2D case) of potential part of the field, a symmetric arcade, is the same plane of symmetry $x = 0$.

Then we add a pair of smaller 'charges' $q_1 = \pm 1$ located at $x = \pm 3$, $z = -3$ as 'parasitic' polarities. The new field line pattern shown in Fig. 6b demonstrates the appearance of two lateral loci of dips. They can be associated with filament barbs (Aulanier & Démoulin 1998; Chae et

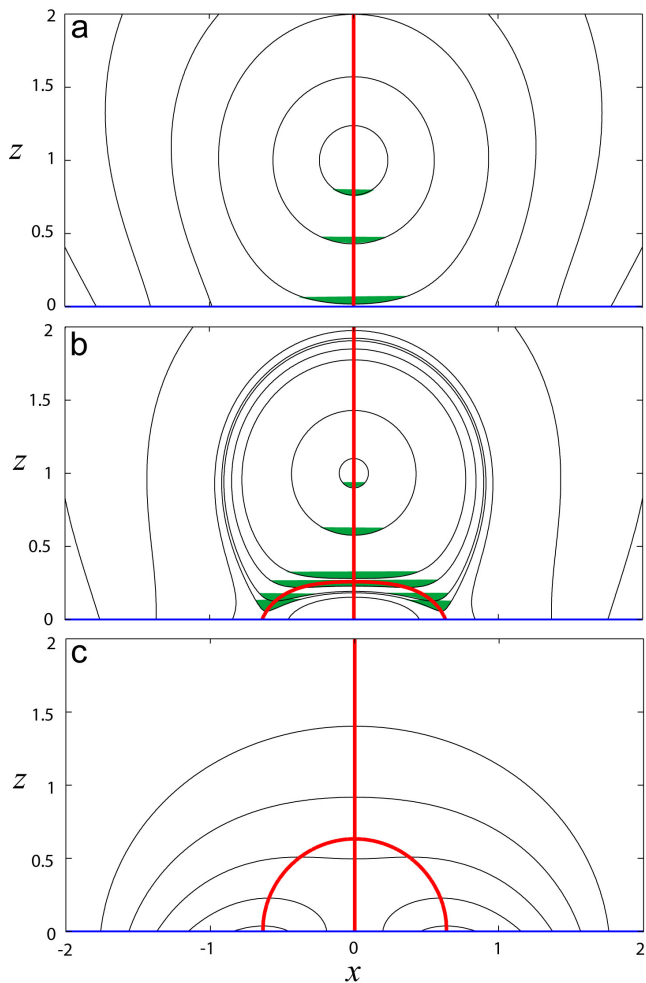


Figure 6. Field lines of a coronal current in equilibrium in a bipolar field (a), in a bipolar field with a presence of parasitic polarities (b), field lines of the potential of the field shown in (b). Thick (red) lines represent neutral lines $B_z = 0$. Shaded (green) areas show possible locations of dense plasma in dips.

al. 2005). The new neutral line is anchored in photospheric PILs between major and minor polarities on both sides of the filament and rises into the corona as a flatten arch.

Fig. 6c shows field lines and neutral lines of the potential part of the configuration with minor polarities. The shape of neutral lines in Figs 6b and c is nearly the same, while field lines are, of course, quite different. The arch-like neutral line is anchored at the same points, although its apex is higher than the apex of the arch in Fig. 6b. Obviously, the field-line curvature is directed downward everywhere near the arched potential neutral line in contrast to Fig. 6b, where the neutral line is the locus of dips. Nevertheless, we believe that the similarity of the neutral surfaces in potential and non-potential fields with the same sub-photospheric sources is the reason for the found tendency for the filament material to gather near the potential-field neutral surface. While the structure of the non-potential field in the corona is quite different from the structure of the potential field, it is sub-photospheric sources of the coronal magnetic field that create necessary conditions for plasma accumulation in certain places.

5 DISCUSSION AND CONCLUSIONS

We found that the filament material is distributed in the vicinity of the coronal potential-field neutral surface. In projection on the chromosphere, a filament is enclosed between two PILs, one at a lower height close to the chromosphere and one at a higher level, which can be considered as a height of the filament spine. Observations of the same filament on the limb by the *STEREO* spacecraft confirm that the height of the spine is really very close to the value obtained from the PIL and filament border matching. Such matching can be used for filament height estimations in the case of absence of limb observations. First attempts of filament height estimations on the disk using neutral surface calculations were made by Zagnetko et al. (2005); Grechnev et al. (2014), and Filippov (2013b).

Of course, the spine height is not constant along the whole length of the filament. We choose the PIL that matches the observed filament spine position over the most part of the length. The height of this PIL can be considered as the most probable or averaged height of the spine. The lower side of the filament is outlined by a low-lying PIL. Filament barbs are housed within protruding sections of the PIL. However not all PIL protrusions are filled with filament barbs. These PIL protrusions show magnetic peninsulas of parasitic polarity on the side of the filament with the dominating polarity. Ends of filament barbs touch the low-lying PIL in accordance with results of Wang (1999, 2001), Chae et al. (2005), and Lin et al. (2005).

The main purpose of this paper is to show that the filament material is located close to the coronal magnetic neutral surface. According to this purpose we selected rather wide filaments with developed barbs located close to the central meridian. Unfortunately, the *STEREO* spacecrafts were not in the best positions for observations of these filaments at the limb. It needed from 2 to 4 days for the filaments to appear at the limb in the field of view of *STEREO*. During this period of time the filaments could slightly change their shapes and heights. This is possibly the major reason of the mismatch between height estimations by the PIL-method and the *STEREO* observations, which reaches about 20% in some selected examples. Study of prominence heights before eruptions (Sterling et al. 2011; Joshi & Srivastava 2011; Filippov 2013a; McCauley et al. 2015) showed that the height changes slowly for several days within 20% mostly due to changes of the prominence shape (appearance and disappearance of particular threads constituting the prominence). Prominences start to rise slowly with the speed of few km s^{-1} or less for several hours before the eruption and then are accelerated fast after reaching the critical height. Filaments and prominences have not exactly the same boundaries in images taken in different wavelengths. Heinzel et al. (2001), Schmieder et al. (2004), Vial et al. (2012) found that some filaments are wider in EUV than in $\text{H}\alpha$. In coronal EUV lines, prominences are observed in absorption and have nearly the same appearance as emitting $\text{H}\alpha$ prominences. Sometimes they suddenly change absorption to emission during activation and eruption (Filippov & Koutchmy 2002). In the Transition Region HeII 304-Å line, prominences look like in $\text{H}\alpha$ coronagraphic images (Romeuf et al. 2007).

However, there is a more principal source of the mis-

match between the data obtained from on-disc and limb observations. Since a filament is not a solid object, different parts of it have different optical thickness in different projections and in different wavelengths. So we compare the heights of not exactly the same spatial elements. Nevertheless, filaments, of course, are quite distinct physical objects although with different visibility in different observations.

All this variations are most probably within the 20% uncertainties that we ascribe to the proposed method of filament height estimation. This accuracy seems enough for the method to be useful for the estimation of filament heights on the disc when there are no observations from other viewpoints. In principle, the accuracy may be higher but it needs more careful study of filaments with better conditions of observations (simultaneous data from two or more viewpoints).

Thus, the filament shape is determined in a first approximation by the shape of the coronal potential-field neutral surface. Obviously, that the flux-rope axis, which is believed to coincide with the filament spine, should be located on the neutral surface. We may not know the detailed structure of the flux rope containing the filament but we can judge where filament barbs are expected to protrude from the filament body, how long and wide could they be. Condition $B_z = 0$ is the necessary condition for the dip existence. At low heights where barb ends are observed, the influence of coronal currents on the B_z distribution is vanishing because of the neighborhood of the rigid photosphere. That is why the shape and position of the potential and non-potential neutral surfaces are very similar (Fig. 6). For this reason the potential magnetic field calculation is a simple and valuable tool for analysis of filament morphological properties. On the other hand, the potential-field decay index distribution can be used for estimation of the filament stability. As any coronal magnetic field extrapolation on the base of only one measured component in the photosphere, our calculations have limited reliability. More accurate calculations on the base of vector magnetic field measurements could confirm or disprove our findings.

ACKNOWLEDGEMENTS

The author thanks the Big Bear Solar Observatory, *STEREO*, *SDO* teams for the high-quality data supplied. This work was supported in part by the Russian Foundation for Basic Research (grant 14-02-92690).

REFERENCES

- Antiochos S. K., Dahlburg R. B., Klimchuk J. A., 1994, *ApJ*, 420, L41
- Aulanier G., Démoulin P., 1998, *A&A*, 329, 1125
- Aulanier G., Démoulin P., van Driel-Gesztelyi L., Mein P., Deforest C., 1998, *A&A*, 335, 309
- Aulanier G., Démoulin P., Mein N., van Driel-Gesztelyi L., Mein P., Schmieder B., 1999, *A&A*, 342, 867.
- Aulanier G., DeVore C. R., Antiochos S. K., 2006, *ApJ*, 646, 1349
- Babcock H. W., Babcock H. D., 1955, *ApJ*, 121, 349
- Bommier V., Landi Degl’Innocenti E., Leroy J.-L., Sahal-Brechot S., 1994, *Sol. Phys.*, 154, 231
- Bommier V., Leroy J. L., 1998, in Webb D., Rust D., Schmieder B., eds, *ASP Conf. Ser. Vol. 150, IAU Colloq. 167: New Perspectives on Solar Prominences*, Astron. Soc. Pac., San Francisco, p. 434
- Chae J., Wang H., Qiu J., Goode P. R., Strous L., Yun H. S., 2001, *ApJ*, 560, 476
- Chae J., Moon Y.-J., Park Y.-D., 2005, *ApJ*, 626, 574
- d’Azambuja M., d’Azambuja L., 1948, *Ann. Observ. Paris, Meudon* 6, Fasc. VII
- DeVore C. R., Antiochos S. K., 2000, *ApJ*, 539, 954
- Filippov B. P., 2011, *Astron. Rep.*, 55, 541
- Filippov B., 2013a, *ApJ*, 773, 10
- Filippov B., 2013b, *Sol. Phys.*, 283, 401
- Filippov B., 2015a, *Astron. Rep.* (in press)
- Filippov B., 2015b, *Geomagnetism & Aeronomy* (in press)
- Filippov B. P., Den O. G., 2000, *Astron. Lett.*, 26, 322
- Filippov B. P., Den O. G., 2001, *J. Geophys. Res.*, 106, 25177
- Filippov B., Koutcmy S., 2002, *Sol. Phys.*, 208, 283
- Filippov B. P., Gopalswamy N., Lozhechkin A. V., 2001, *Sol. Phys.*, 203, 119
- Filippov B. P., Gopalswamy N., Lozhechkin A. V., 2002, *Astron. Rep.*, 46, 417
- Gibson S. E., Fan Y., 2006, *J. Geophys. Res.*, 111, A12103
- Grechnev V. V., Uralov A. M., Slemzin V. A., Chertok I. M., Filippov B. P., Rudenko G. V., Temmer, M., 2014, *Sol. Phys.*, 289, 289
- Heinzel P., Schmieder B., Tziotziou K., 2001, *ApJL*, 561, L223
- Howard R. F., Harvey J. W., 1964, *ApJ*, 139, 1328
- Howard R. A. et al., 2008, *Space Sci. Rev.*, 136, 67
- Ioshpa B. A., 1968, in Kippenheuer K.O., ed., *IAU Symp. 35: Structure and Development of Solar Active Region*, D. Reidel, Dordrecht, p. 261
- Joshi A. D., Srivastava N., 2011, *ApJ*, 730, 104
- Kim I. S., 1990, in Ruzdjak V., Tandberg-Hanssen E., eds, *Dynamics of Quiescent Prominences, Lecture Notes in Physics, Vol. 363*, Springer, Berlin, p. 49
- Kippenhahn R., Schlüter A., 1957, *Z. Astrophys.*, 43, 36
- Kuperus M., Raadu M. A., 1974, *A&A*, 31, 189
- Leroy J. L., 1977, *A&A*, 60, 79
- Leroy J. L., 1978, *A&A*, 64, 247
- Lin Y., Wiik J. E., Engvold O., Rouppe van der Voort L., Frank Z. A., 2005, *Sol. Phys.*, 227, 283
- Mackay D. H., Karpen J. T., Ballester J. L., Schmieder B., Aulanier G., 2010, *Space Sci. Rev.*, 151, 333
- McCauley P. I., Su Y. N., Schanche N., Evans K. E., Su C., McKillop S., Reeves K. K., 2015, *Sol. Phys.*, 290, 1703
- Martin S. F., 1998, *Sol. Phys.*, 182, 107
- Martin S. F., Echols C. R., 1994, in Rutten R. J., Schrijver C. J., eds, *Solar Surface Magnetism*, Kluwer, Dordrecht, p. 339
- Martin S. F., Bilimoria R., Tracadas P. W., 1994, in Rutten R. J., Schrijver C. J., eds, *Solar Surface Magnetism*, Kluwer, Dordrecht, p. 303
- McIntosh P. S., 1972, *Rev. Geophys. Space Phys.*, 10, 837
- Molodenskii M. M., Filippov B. P., 1987, *Soviet Astron.*, 31, 564
- Parenti S., 2014, *Living Rev. Solar Phys.*, 11, 1
- Plocieniak S., Rompolt B., 1973, *Sol. Phys.*, 29, 399
- Pneuman G. W., 1983, *Sol. Phys.*, 88, 219
- Priest E. R., Forbes T. G., 1990, *Sol. Phys.*, 126, 319

- Priest E. R., Hood A. W., Anzer U., 1989, *ApJ*, 344, 1010
Romeuf D., Meunier N., Noëns J.-C., Koutchmy S., Jimenez R., Wurmser O., Rochain S., 'Observateurs Associés' Team, 2007, *AA*, 462, 731
Rompolt B., 1990, *Bull. Hvar Obs.* 14, 37
Rust D. M., 1967, *ApJ*, 150, 313
Rust D. M., Kumar A., 1994, *Sol. Phys.*, 155, 69
Schmieder B., Lin Y., Heinzel P., Schwartz P., 2004, *Sol. Phys.*, 221, 297
Schou, J. et al., 2012, *Sol. Phys.*, 275, 229
Smith S. F., Ramsey H. E., 1967, *Sol. Phys.*, 2, 158
Sterling A. C., Moore R. L., Freeland S. L., 2011, *ApJL*, 731, L3
Tandberg-Hanssen E., 1970, *Sol. Phys.*, 15, 359
Tandberg-Hanssen E., 1974, *Solar Prominences, Geophysics and Astrophysics Monographs* 12, D. Reidel, Dordrecht.
van Ballegoijen A. A., 2004, *ApJ*, 612, 519
van Ballegoijen A. A., Martens, P. C. H., 1989, *ApJ*, 343, 971
van Tend W., Kuperus M., 1978, *Sol. Phys.*, 59, 115
Vial J.-C., Olivier K., Philippon A. A., Vourlidas A., Yurchyshyn V., 2012, *AA*, 541, A108
Wang Y.-M., 1999, *ApJ*, 520, L71
Wang Y.-M., 2001, *ApJ*, 560, 456
Wuelser J.-P. et al., 2004, in Fineschi S, Gummin M. A., eds, *Proc. SPIE Conf. Ser. Vol. 5171, Telescopes and Instrumentation for Solar Astrophysics*. SPIE, Bellingham, p. 111
Zirin H., Severny A., 1961, *The Observatory*, 81, 155
Zagnetko A. M., Filippov B. P., Den O. G., 2005, *Astron. Rep.* 49, 425

This paper has been typeset from a $\text{T}_{\text{E}}\text{X}/\text{L}^{\text{A}}\text{T}_{\text{E}}\text{X}$ file prepared by the author.